Title
Organization of the cytoskeleton in early Drosophila embryos.

Journal
The Journal of cell biology, 102(4)

ISSN
0021-9525

Authors
Karr, TL
Alberts, BM

Publication Date
1986-04-01

DOI
10.1083/jcb.102.4.1494

Peer reviewed

Organization of the Cytoskeleton in Early *Drosophila* Embryos

Timothy L. Karr and Bruce M. Alberts

Department of Biochemistry and Biophysics, University of California, San Francisco, California 94143

Abstract. The cytoskeleton of early, non-cellularized *Drosophila* embryos has been examined by indirect immunofluorescence techniques, using whole mounts to visualize the cortical cytoplasm and sections to visualize the interior. Before the completion of outward nuclear migration at nuclear cycle 10, both actin filaments and microtubules are concentrated in a uniform surface layer a few micrometers deep, while a network of microtubules surrounds each of the nuclei in the embryo interior. These two filament-rich regions in the early embryo correspond to special regions of cytoplasm that tend to exclude cytoplasmic particles in light micrographs of histological sections. After the nuclei in the interior migrate to the cell surface and form the syncytial blastoderm, each nucleus is seen to be surrounded by its own domain of filament-rich cytoplasm, into which the cytoskeletal proteins of the original surface layer have presumably been incorporated. At interphase, the microtubules seem to be organized from the centrosome directly above each nucleus, extending to a depth of at least 40 μm throughout the cortical region of cytoplasm (the periplasm). During this stage of the cell cycle, there is also an actin "cap" underlying the plasma membrane immediately above each nucleus. As each nucleus enters mitosis, the centrosome splits and the microtubules are rearranged to form a mitotic spindle. The actin underlying the plasma membrane spreads out, and closely spaced adjacent spindles become separated by transient membrane furrows that are associated with a continuous actin filament–rich layer. Thus, each nucleus in the syncytial blastoderm is surrounded by its own individualized region of the cytoplasm, despite the fact that it shares a single cytoplasmic compartment with thousands of other nuclei.

THE early events in *Drosophila* embryogenesis that lead up to gastrulation have been extensively studied (8, 29, 37, 41, 52). After fertilization and the completion of meiosis, the early nuclear divisions form a syncytium; cellularization occurs later after the nuclei have divided thirteen times. Until nuclear cycle 7, all of the nuclei are located in the interior of the embryo. The nuclei then migrate outward to the egg periphery during nuclear cycles 8 and 9, with most arriving at the surface to form a monolayer just beneath the egg plasma membrane early in interphase of cycle 10 (a few "pole cell nuclei" reach the posterior end of the egg during nuclear cycle 9). After four more, nearly synchronous nuclear divisions in this "syncytial blastoderm" state, cellularization begins synchronously during early cycle 14 (11, 30, 31). Gastrulation commences later in cycle 14, shortly after a monolayer of cells has formed (reviewed in Fig. 1 of reference 8).

Important developmental events occur in early *Drosophila* embryos after the nuclei reach the embryo periphery. Although initially identical, the nuclei appear to become different in their transcriptional patterns by cycle 13 (12), and they are incorporated into cells at cycle 14 that are determined to form a particular larval segment (21, 43). Ligation experiments performed on embryos before this time suggest that the positional information that specifies segmental determination develops gradually in the syncytial embryo (26, 44). It therefore seems likely that at least some of the factors that inform the nuclei of their location in the embryo become highly localized in the cytoplasm during the syncytial blastoderm stage of development (nuclear cycles 10–14).

Recently, Warn et al. (48) have described actin filament distributions in *Drosophila* embryos during the syncytial blastoderm stages. These studies demonstrated that actin filaments are localized in domains above each somatic nucleus, closely associated with the plasma membrane, and that these actin "caps" undergo cycle-specific reorganizations during each mitosis in the syncytial blastoderm. In addition, myosin was observed to co-localize with plasma membrane–associated actin during cellular blastoderm formation (47). Our laboratory has begun investigating the behavior of all of the major cytoskeletal elements during early development with the hope of integrating the structure and function of the cytoskeleton into the overall picture of embryogenesis. As a starting point, we have characterized the distribution of actin- and tubulin-containing structures in early embryos by immunofluorescent staining.

Materials and Methods

Reagents

Pipes, EGTA, Triton X-100, β-mercaptoethanol, bovine serum albumin (BSA),

and the DNA-specific dyes 4,6 diamidino-2-phenylindole (DAPI)[1] and (2-[2-(4-hydroxyphenyl)-6-benzimidazoyl]-6-[1-methyl-4-piperazyl]benzimidazole (Hoechst 33258) were obtained from Sigma Chemical Co. (St. Louis, MO). Mowiol 4.88 was purchased from Hoechst, Germany. An aqueous solution that contains 20% formaldehyde from Polysciences Inc. (Warrington, PA) was used as a fixative. Taxol was a gift from Dr. M. Suffness, National Cancer Institute.

Buffers

Phosphate-buffered saline (PBS) contained per liter; 8 g NaCl, 0.2 g KCl, 0.2 g KH_2PO_4, 1.15 g Na_2HPO_4, adjusted to pH 7.3 with NaOH. Embryos were fixed in a buffer that contained 0.1 M Pipes, 1 mM $MgCl_2$, and 1 mM EGTA, adjusted to pH 6.9 with KOH (designated PEM buffer). Sodium dodecyl sulfate (SDS) sample buffer was 62 mM Tris-Cl (pH 6.8) that contained 5% β-mercaptoethanol, 10% glycerol, and 3% SDS.

Antibodies

Anti-tubulin and anti-actin mouse monoclonal antibodies were a gift from Dr. S. Blose (1). Rabbit anti-actin polyclonal serum was purchased from Miles Laboratories, Inc. (Naperville, IL) and affinity purified as described below. Rhodamine-labeled goat anti-mouse IgG and rhodamine-labeled goat anti-rabbit IgG were purchased from Cappel Laboratories (Cochranville, PA). Fluorescein-labeled goat anti-mouse IgG was obtained from Litton Bionetics (Kensington, MD). All three fluorescent antibodies were pre-treated as described below before application to fixed embryos.

Permeabilization and Fixation Protocol

Embryos from *Drosophila melanogaster* (Oregon R) flies were collected at 25°C on apple juice/agar plates at timed intervals, essentially as described by Elgin and Miller (7). All subsequent manipulations were done at 22°C. Embryos were gently dislodged from collection plates by rinsing with a solution that contained 0.4% NaCl and 0.03% Triton X-100, collected on 120-μm nylon screening, rinsed thoroughly, and then transferred to a 50% commercial bleach solution (active ingredient 2.6% sodium hypochlorite) for 90 s to remove the chorion. De-chorionated embryos were extensively washed with the NaCl/Triton rinse solution and transferred into 5 ml of PEM buffer in a 15-ml screw cap tube. Taxol (10 μl of a 0.5 mM solution in dimethylsulfoxide) was added, followed by 5 ml of heptane (in the text, concentrations of taxol are given as if it distributes evenly into the entire 10 ml). After shaking vigorously for 30 s, 1 ml of 20% formaldehyde was added, and shaking was resumed for an additional 10 min (on a New Brunswick model G2 platform shaker [New Brunswick Scientific Co., Inc., Edison, NJ] operating at 350 rpm). The fixed embryos were collected on nylon screening, washed briefly in PBS, and transferred to a round bottom flask that contained 10 ml of heptane and 10 ml of 90% methanol that contained 10% H_2O and 0.05 M Na_3EGTA previously cooled to −70° with dry ice (25). After agitating vigorously for 10 min, the contents of the flask were rapidly warmed to room temperature under a stream of hot tap water with gentle swirling. This procedure effectively removes the vitelline membrane from most of the embryos (25). The devitellinized embryos were transferred into test tubes, rinsed three times with the methanol solution, re-hydrated by passage through a solution of 50/50 methanol/PBS, and finally transferred into PBS. Light microscopic visualization of plastic sections reveals that these fixation methods leave the overall structure of the embryonic cytoplasm intact, with no indication of gross changes.

Indirect Immunofluorescent Staining of Whole Fixed Embryos

Approximately 300–500 embryos prepared as described above were placed in a 1-ml test tube and incubated with 0.5 ml of a PBS solution that contained 1% BSA and 0.1% Triton X-100 for 0.5 h, using gentle rotation to invert the tube every 20 s to ensure proper mixing. All succeeding antibody incubations and rinses were done in this PBS solution that contained BSA and Triton at 22°C. The embryos were next incubated with ~5–10 μg/ml of the desired antibody for 1 h, followed by rinsing for at least 2 h more. Embryos were then stained for 1 h with either a goat anti-mouse or a goat anti-rabbit IgG coupled to rhodamine or fluorescein, followed by a 2-h rinse. Finally the embryos were transferred into PBS that contained either 1 μg/ml Hoechst 33258 (14) or DAPI (32) for 4 min and then rinsed for 1 h in PBS without Triton. For viewing, embryos were mounted in Mowiol 4.88 under 22 × 30-mm coverslips (28).

[1] *Abbreviations used in this paper:* DAPI, 4,6 diamidino-2-phenylindole; Hoechst 33258, (2-[2-(4-hydroxyphenyl)-6-benzimidazoyl]-6-[1-methyl-4-piperazyl]-benzimidazole.

Light Microscopy

Stained embryos were examined using either a Nikon Diaphot or Zeiss standard microscope equipped with epifluorescence optics. Rhodamine, fluorescein, and Hoechst 33258 or DAPI fluorescence were observed using Nikon G, B, and UV filter cassettes, respectively, or Zeiss filter cassettes 01, 10, or 15. A Zeiss Plan-Neofluar 25/0.8, a Zeiss Plan-Neofluar 100/1.3, or a Leitz Plan-apo 63/1.4 were used as the primary objective lenses. A Nikon FE or Zeiss M35 camera and Kodak 2415 technical pan film were used to record the images obtained. Negatives were developed with Diafine.

Preparation of Fluorescently Labeled Secondary Antibodies for Embryo Staining

Before staining embryos with either fluorescein-labeled or rhodamine-labeled goat anti-mouse or goat anti-rabbit IgG antibodies, the following procedures were done. Labeled antibodies, received as a lyophilized powder, were resuspended in water as per instructions, and then further diluted three times in PBS to a final concentration of ~10–20 mg/ml. This solution (3 ml) was mixed at room temperature with 0.5 g of rabbit liver acetone powder (Gibco, Grand Island, NY) and warmed to 37°C for 2 h with constant mixing. After an overnight incubation at 4°C, the suspension was centrifuged for 10 min at 10,000 *g* and the supernatant was decanted, passed through a 0.45-μm Millipore filter, and stored at −70°C. Further preadsorption to embryos is necessary before these antibodies can be used for staining embryos. An aliquot of antibody prepared as described above was thawed and diluted ten times into PBS. The diluted antibody was then incubated for 1–2 h at room temperature with ~0.1 g of fixed embryos per ml of antibody solution. After this treatment, the embryos were allowed to settle, and the supernatant was decanted and passed again through a 0.45-μm Millipore filter. These antibodies were stored at 4°C in sterile vials and diluted an additional twenty to thirty times for immunofluorescent staining.

Recently we have used affinity-purified goat anti-mouse and goat anti-rabbit fluorescent labeled antibodies from Cappel Laboratories and Jackson Laboratory (Bar Harbor, ME) that require only the pre-adsorption to fixed embryos before use. The poor immunofluorescent staining of actin structures using commercial anti-actin sera necessitated their affinity purification on G-actin columns. A 1-ml column of Affigel 10 (Bio-Rad Laboratories, Richmond, CA) that contained ~1 mg of rabbit G-actin (a gift from Dr. K. Miller) was constructed, and ~40–50 mg of anti-actin sera applied. After an extensive wash with PBS, bound antibodies were eluted with 4.5 M $MgCl_2$ that contained 2.5 mg/ml BSA. 1-ml fractions were collected, dialyzed against PBS, and used directly for immunofluorescence experiments.

When embryos were treated with either rabbit pre-immune sera or supernatant that contained non-immune IgGs from a mouse myeloma cell line, subsequent staining with secondary antibodies failed to reveal any staining of cytoskeletal structures (data not shown). Appropriate controls for double label immunofluorescence experiments were also done that showed no detectable cross-reactivity between the fluorescently labeled secondary IgGs and the inappropriate heterologous antibody.

Plastic Embedding and Sectioning of Embryos

Embryos from timed collections were fixed and stained with rhodamine-labeled secondary antibody to reveal either actin or tubulin structures as described above. To ensure penetrance of primary and secondary antibodies into the interior, both the amount of antibodies and the incubation times were increased by fivefold. However, the optimal conditions for visualizing interior microtubule and actin structures had to be determined empirically, since these conditions can vary with the fixation and the quality and purity of the antibodies used. The stained embryos were treated with 1 μg/ml DAPI in PBS for 5 min, rinsed for 15 min in PBS, transferred directly into 100% ethanol, and resuspended in 100% ethanol after settling. After being exposed to ethanol for a further 5 min, the dehydrated embryos were transferred into a mixture of 80% EPON/20% propylene oxide at 22°C, allowed to settle for ~5 min, and then resuspended in the same solution. The embryos were then transferred into a 90% EPON/10% propylene oxide mixture, allowed to settle, and resuspended. Finally, the embryos were transferred into 100% EPON for 10 min, placed in sectioning capsules, and centrifuged gently in a table-top centrifuge to pack the embryos in the tip of the capsule. After treatment at 60°C for 36 h to harden the plastic, 1–5-μm thick sections were cut with a glass knife on a Sorvall MT-2 ultramicrotome. The sections were transferred to microscope slides, dried, and mounted in Mowiol 4.88 under coverslips for examination with epifluorescence optics.

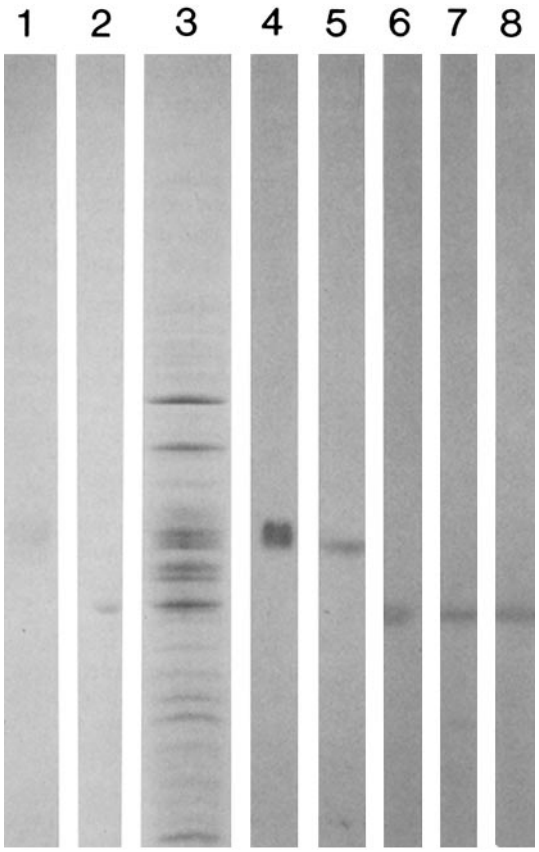

Figure 1. Demonstration of the monospecific reactivity of actin and tubulin antibodies to *Drosophila* embryo proteins. Proteins were separated by SDS polyacrylamide gel electrophoresis as described in Materials and Methods. A Coomassie Blue–stained 8% polyacrylamide gel showing the proteins blotted onto nitrocellulose filters is shown in lane *1* (purified mammalian tubulin), lane *2* (purified mammalian actin), and lane *3* (crude *Drosophila* embryo extract). Lanes *4–8* are autoradiographs of strips of nitrocellulose incubated with one primary antibody and then washed and probed with either sheep anti-mouse ^{125}I-IgG or a sheep anti-rabbit ^{125}I-IgG, as appropriate. Lanes *5*, *7*, and *8* contained *Drosophila* embryo proteins and lanes *4* and *6* contained mammalian tubulin and actin, respectively. These lanes were probed with the following primary antibodies: lanes *4* and *5*, mouse anti-tubulin; lanes *6* and *7*, rabbit anti-actin; lane *8*, mouse anti-actin.

SDS Polyacrylamide Gel Electrophoresis and Immunoblot Analysis

Total *Drosophila* proteins were extracted from dechorionated embryos by homogenization in hot SDS sample buffer and heating to 100°C for 10 min. After these proteins were electrophoresed through 8% SDS polyacrylamide gels (20), they were transferred to nitrocellulose paper by blotting for 48 h (40). The nitrocellulose blots were treated for 30 min with either affinity-purified rabbit anti-actin, mouse anti-actin, or mouse anti-tubulin antibodies. Primary antibody probes were removed and the blots washed extensively with 0.1% Triton X-100 in PBS for 1 h. The appropriate ^{125}I-labeled goat anti-mouse or goat anti-rabbit secondary antibody diluted in PBS/Triton that contained 1% BSA was applied (500,000 cpm per blot). Finally, the nitrocellulose blots were rinsed and washed extensively in PBS/Triton, dried, and exposed to Kodak XAR-5 x-ray film for 3 d at −70°C.

Results

We have examined the cytoskeleton in *Drosophila* embryos by indirect immunofluorescent staining. Since the antibodies used had been prepared against mammalian antigens, immunoblot analyses were performed to determine their reactivity against whole *Drosophila* embryo extracts. In the experiment shown in Fig. 1, the total proteins in a *Drosophila* embryo extract, as well as bovine brain microtubule protein and rabbit muscle actin controls, were resolved by SDS-polyacrylamide gel electrophoresis and then transferred to a nitrocellulose filter. Comparison of the reactivity of these filters with the various antibodies demonstrates that a single major protein band in the *Drosophila* extract is recognized in each case (lanes *5*, *7*, and *8*). This band co-migrates with either authentic actin (lane *6*) or tubulin (lane *4*), as appropriate for the particular antibody tested. We conclude that the three antibodies used for our studies react with the designated target antigens in *Drosophila*.

For our cytological studies, we have used a modification of methods developed by Mitchison and Sedat (25) for the formaldehyde fixation and de-vitellinization of whole *Drosophila* embryos. The major modification used is the addition of 0.5 μM taxol, a plant-derived microtubule-stabilizing drug, to the buffer/heptane mixture for 30 s before the addition of formaldehyde.

The effect of taxol on the visualization of microtubule-containing structures in *Drosophila* embryos is dramatically shown in Fig. 2, *a* and *b*, where micrographs of two embryos that were fixed and prepared for immunofluorescence in parallel are shown. Both embryos were fixed during metaphase of nuclear cycle 11, as determined by their DNA staining patterns (not shown), but only the embryo in Fig. 2*b* was treated with taxol. Whereas the taxol-treated embryo displays numerous mitotic spindles of the expected morphology, the embryo fixed without taxol present (Fig. 2*a*) reveals no distinguishable microtubule-containing structures.

The bottom panels in Fig. 2 show a small region of the syncytial blastoderm surface that contains nuclei in slightly different stages of anaphase. The arrows point to corresponding microtubule (Fig. 2*c*) and DNA structures (Fig. 2*d*) at two different stages of anaphase chromosome movement. Inspection of the two mitotic figures reveals that microtubules grow rapidly from the centrosome during anaphase, as commonly observed in other systems (3). Control experiments, described in the Discussion, suggest that taxol is stabilizing pre-existing microtubules under our conditions rather than inducing new ones, and the consistent correlation of spindle and aster structures with the stage of mitosis supports this view. We therefore believe that the microtubule structures found during interphase (see below), which likewise depend on taxol treatment for their preservation, represent structures that are pre-existing in the embryo.

Actin and Tubulin Form an Extensive Cortical Network in Early Embryos That Is Not Perturbed by Mitosis

Examination of actin and tubulin distributions in cycle 1–8 embryos, before the arrival of nuclei at the surface, reveals an extensive cortical network of these two proteins. Fig. 3 shows representative examples, panels *a*, *c*, and *e* being views of embryos stained to reveal tubulin, and panels *b*, *d*, and *f* being corresponding views of embryos stained to reveal actin. The low power views show a global distribution of both actin and tubulin over the entire embryo surface. At higher magnification, microtubules appear to form a filamentous network (Fig. 3*c*), whereas a punctate actin pattern is seen (Fig.

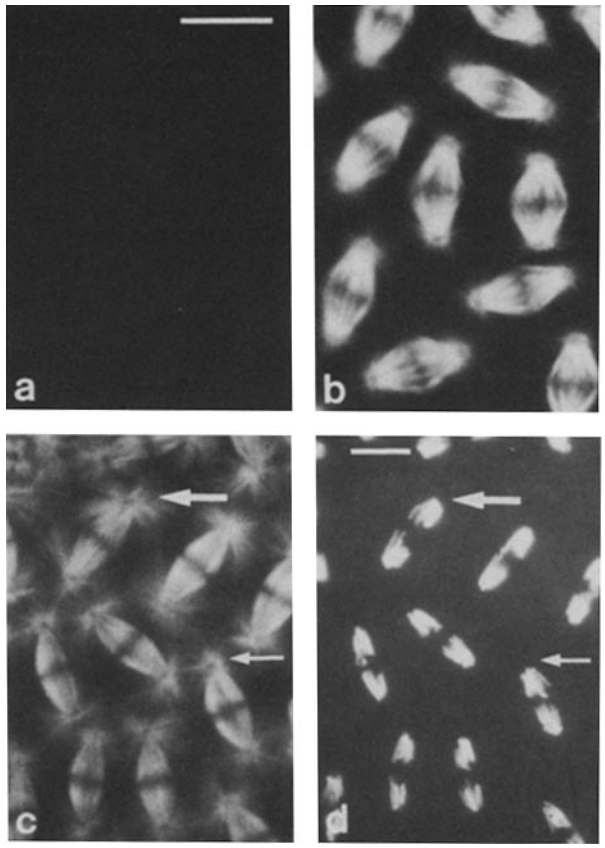

Figure 2. Taxol preservation of microtubule structures in mitotic spindles. Embryos were fixed in the absence (*a*) or presence (*b*, *c*, and *d*) of 0.5 μM taxol and then stained to reveal microtubule and DNA structures as described in Materials and Methods. *a* and *b* show the striking effect of taxol on a cycle 11 embryo (bar, 10 μm); the metaphase state of both embryos was determined by examining the chromosomes, which were stained with Hoechst 33258 (not shown). The exposure times used for photography were identical, and prints were developed using the same contrast paper and exposure times. *c* and *d* display the microtubule structures and the DNA, respectively, in a small region of a doubly labeled stage 12 embryo that contained mitotic figures varying slightly in their extent of anaphase chromosomal movement, as part of a general mitotic gradient best seen in lower magnification views (bar, 10 μm). The arrows in *c* and *d* serve as reference points for comparing astral microtubules at different times of anaphase: in *c*, the larger arrow points to an aster from a spindle at a later stage of anaphase than the spindle denoted by the smaller arrow, with the nuclei being staged by the distance that separated their chromosomes in *d*.

3*d*). Views of sectioned embryos show that both the cortical tubulin (Fig. 3*e*) and actin (Fig. 3*f*) extend below the plasma membrane to a depth of ~3–4 μm.

The migration of the nuclei outward toward the embryo cortex appears to begin in late nuclear cycle 7 embryos, with most movement occurring stepwise during telophase of cycles 7, 8, and 9 (8). When embryos in metaphase of nuclear cycle 7 are stained to reveal microtubules, the metaphase spindles can be seen beneath the surface, while the cortical layer of microtubules remains indistinguishable from the network found in all earlier embryos (not shown). Thus, in these early embryos the cortical layer of microtubules does not appear to be altered in the transition from interphase to mitosis (see also Fig. 4*a*, below).

As the Nuclei Reach the Surface of the Egg, the Cortical Cytoplasm Becomes Partitioned into Domains Rich in Cytoskeletal Elements That Are Organized Around Each Nucleus

Each interphase nucleus in the interior of the early embryo is closely surrounded by a special cytoplasmic domain of microtubules. These microtubules form a radiating network of filaments around each nucleus, as illustrated by the view of the sectioned cycle 9 embryo shown in Fig. 3*e*.

Similar observations of embryos fixed during various stages suggest that each outward-migrating nucleus begins to influence the network of cortical microtubules when it reaches the embryo surface. For example, in the late cycle 8 embryos shown in Fig. 4, the future pole cell nuclei with their associated microtubules have entered the cortical region at the posterior end of the embryo. As shown in both low (Fig. 4*a*) and high (Fig. 4*c*) magnification views that focus on the surface, there is a decrease in the cortical microtubule density in areas immediately above the out-of-focus nuclei (shown in focus just below the surface in Fig. 4, *b* and *d*).

When the remaining nuclei (which will form the somatic tissues) approach the embryo surface about one nuclear division cycle later, they complete a global reorganization of the cortical cytoplasm. Fig. 5 presents photographs that illustrate successive stages in this process, using triple-label staining for actin, tubulin, and DNA. Each row is labeled according to the nuclear cycle stage of the embryo, as determined by the DNA stain. We estimate that the four embryos shown span a total of 2–3 min of development time (8), during which the nuclei move outward ~10–12 μm (these nuclei are ~12, 9, 5, and 2 μm from the surface, respectively). In the youngest embryo (top row), a network of microtubules is located directly above each migrating nucleus, ~8–10 μm below the (out-of-focus) cortical layer of microtubules. At this time, no perturbation in the cortically disposed actin network is detected, and no actin is visible around the migrating nuclei.

The microtubules around each nucleus begin to intermingle with the network of microtubules in the cortex in telophase of cycle 9, but an extensive invasion of microtubules into the cortex is seen only when interphase of cycle 10 begins. The nuclei are now ~5 μm from the surface (early interphase panel) and most of their microtubules are in the cortical area; no change in the cortical actin is yet apparent. However, by mid-interphase, a dramatic reorganization of the cortical actin into a "cap" directly above each nucleus has begun, and both the cortical actin and the cortical tubulin have been rearranged with respect to the nuclei (bottom row, Fig. 5 and top row of Figs. 6 and 7). By this time, nuclear migration is complete, and ~400 nuclei reside in a monolayer 2 μm below the plasma membrane (8).

In Cycle 10 Embryos, the Distribution of Both Microtubules and Actin Filaments Appear to Follow the Centrosome

The entire duration of cycle 10 is only 9 min, with interphase estimated to occupy about half of the cycle (see Table 2 in reference 8). Fig. 6 displays the tubulin-containing structures in embryos that are slightly older than those shown in Fig. 5, proceeding from mid-interphase through telophase of cycle 10. Fig. 7 shows corresponding views of the actin-containing structures at the same times.

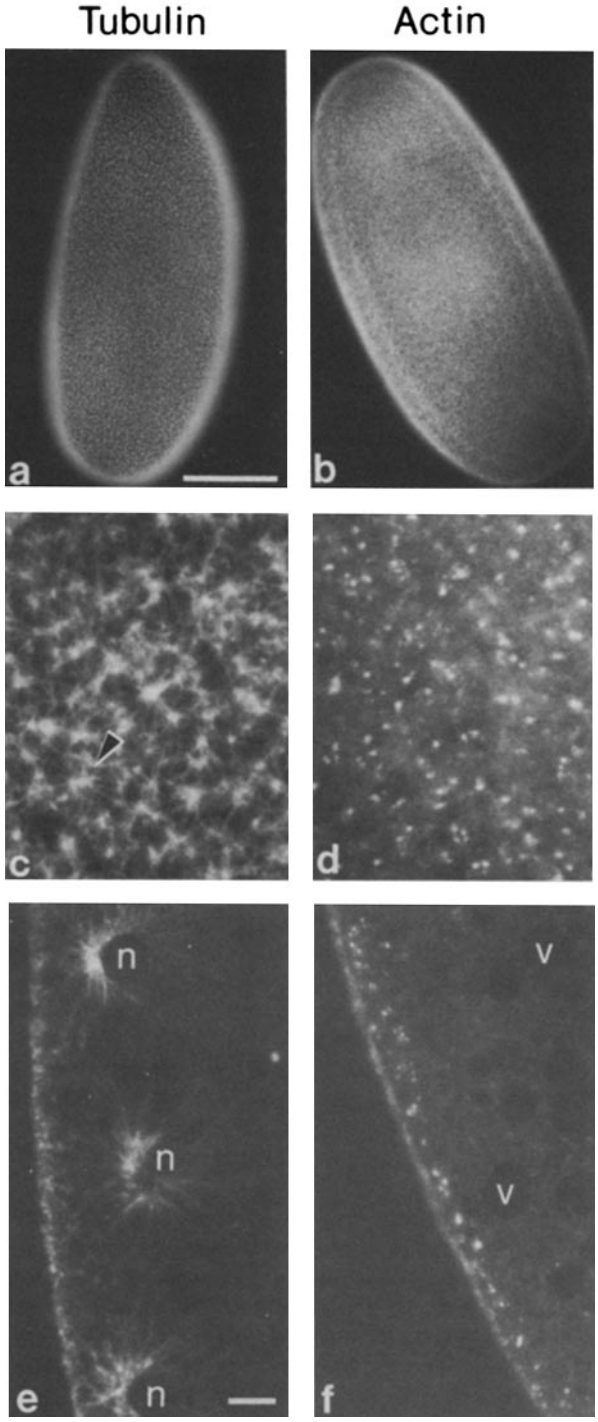

Figure 3. The tubulin and actin patterns present in early *Drosophila* embryos before the completion of nuclear migration. Embryos were fixed, stained, and viewed either in whole mount or in plastic sections, as described in Materials and Methods. The left-hand panels show tubulin staining patterns and the right-hand panels show actin staining patterns. Both low magnification (*a* and *b*) and high magnification (*c* and *d*) surface images of whole mount embryo preparations are shown at nuclear cycle 4. The arrowhead in *c* points to a presumed microtubule organizing center. *e* and *f* show 1-μm thick plastic sections; the embryo in *f* is at nuclear cycle 4 (*v* denotes apparent vacuoles), while the embryo in *e* is in interphase of nuclear cycle 9, which enables us to illustrate the network of microtubules observed around all nuclei before they reach the embryo surface (*n* denotes nuclei). At this stage of nuclear migration, the cortical layer of microtubules is unchanged from the structure seen in all earlier embryos (data not shown). For panels *a* and *b*, the bar denotes 100 μm; the bar in *e* denotes 5 μm for the remaining panels.

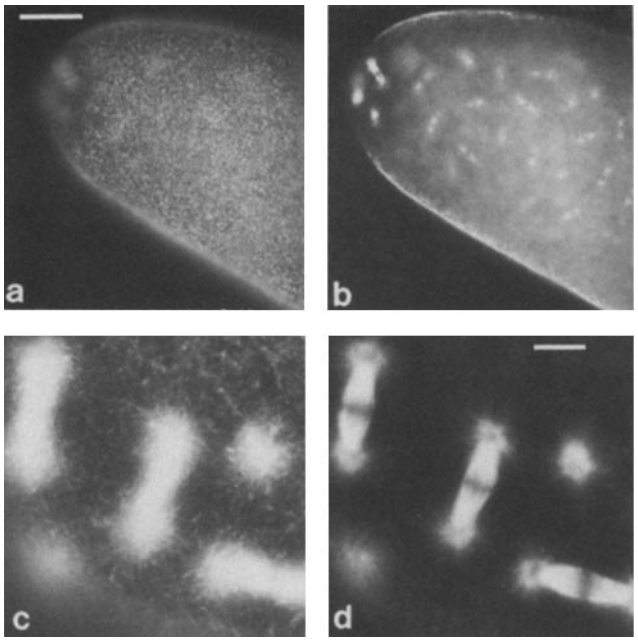

Figure 4. Microtubule structures present during mitosis of nuclear cycle 8. Microtubule structures present at the surface (*a*) and in mitotic spindles present just below the surface (*b*) are shown at two focal planes of a whole mount embryo in mitosis at nuclear cycle 8. The mitotic state of this embryo was assessed by examination of its chromosome structure in DNA-stained images (not shown). *c* and *d* show high magnification views (at two different focal planes) of the posterior end of a similar embryo, revealing the microtubule structures present at the surface and ~5 μm below the surface, respectively. For *a* and *b*, bar denotes 50 μm, for *c* and *d*, bar denotes 10 μm.

The tubulin and actin staining patterns in embryos that we infer to be in mid-to-late interphase of cycle 10 are shown in the top row of Figs. 6 and 7, respectively. The DNA staining patterns (not shown) reveal a nucleus located at the center of each astral array of microtubules (Fig. 6) and immediately below each actin cap (Fig. 7). When viewed at a higher magnification (column *B*), the regions of the cortical cytoplasm that are far away from any nucleus are seen to be nearly free of actin filaments and microtubules. The localized concentration of both actin and tubulin at interphase of cycle 10 suggests that each nucleus in the syncytium organizes its own domain of cytoplasm around it. For different nuclei, this domain could in principle contain different proteins.

Embryos that are 1–2 min older are shown in the prophase panels of Figs. 6 and 7. During prophase, the centrosome, which is located between the nuclear envelope and the plasma membrane early in interphase, splits to create two centrosomes that move to opposite sides of the nucleus (38). The array of microtubules around each nucleus correspondingly splits into two clear halves, as the tubulin begins to be reorganized in preparation for formation of the bipolar mitotic spindle. The actin is found in a similarly bipolar arrangement at prophase, which by double-label staining is seen to match the tubulin polarity (not shown). Thus, both actin and microtubule distributions seem to follow the position of the centrosome in these embryos.

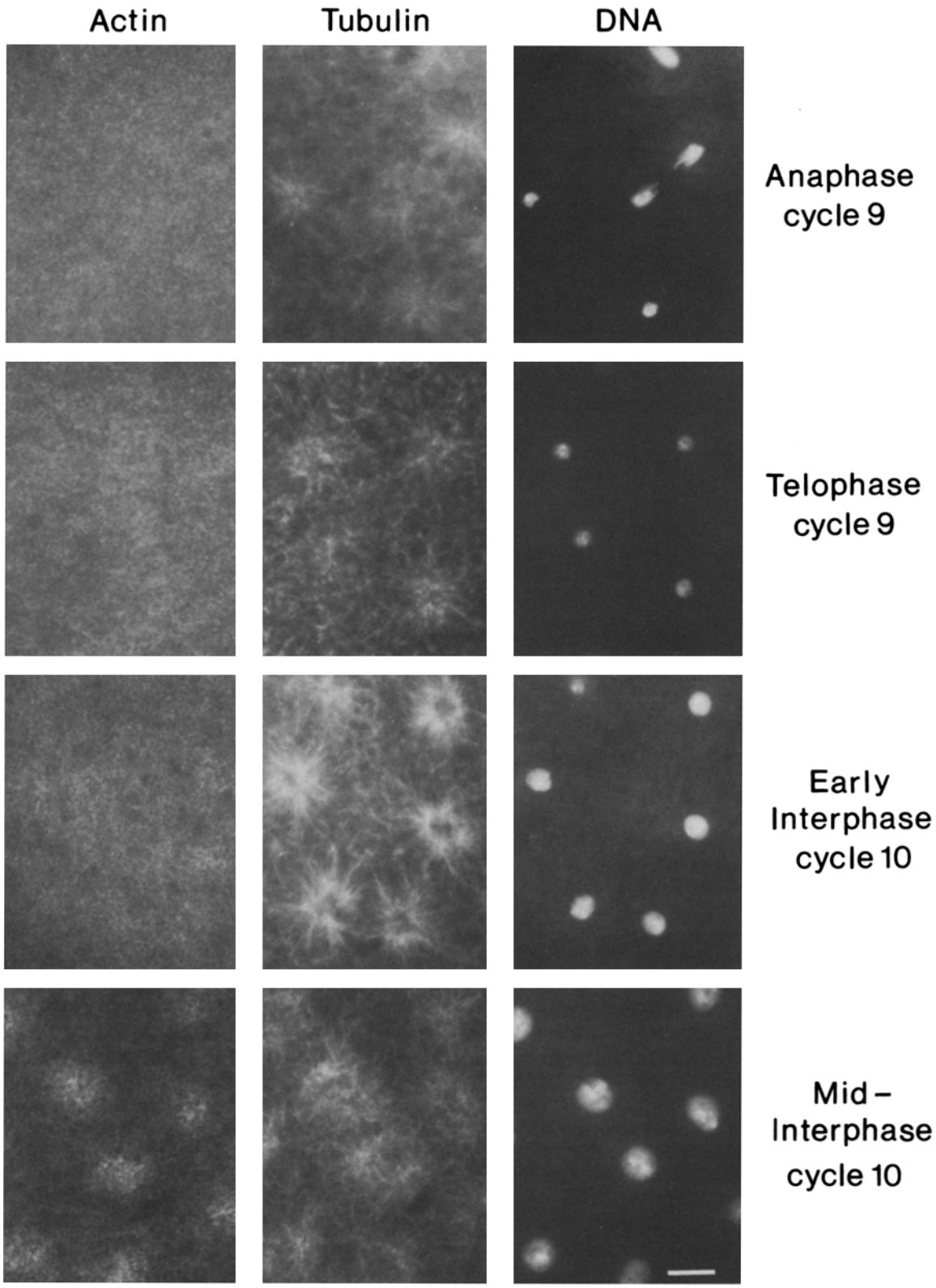

Figure 5. Actin, tubulin, and DNA behavior during late nuclear cycle 9 and early cycle 10. Embryos were fixed and triply stained to reveal actin, tubulin, and DNA structures as described in Materials and Methods, which were photographed using the rhodamine, fluorescein, and ultraviolet filter cassettes, respectively. The four horizontal rows display embryos that were fixed at four successive times during cycles 9 and 10, as labeled on the right. The tubulin images were obtained at focal distances of ~9, 6, 2, and 1 μm below the surface. All of the actin images were photographed at the surface, as there was no detectable actin associated with the advancing nuclei. Bar, 10 μm.

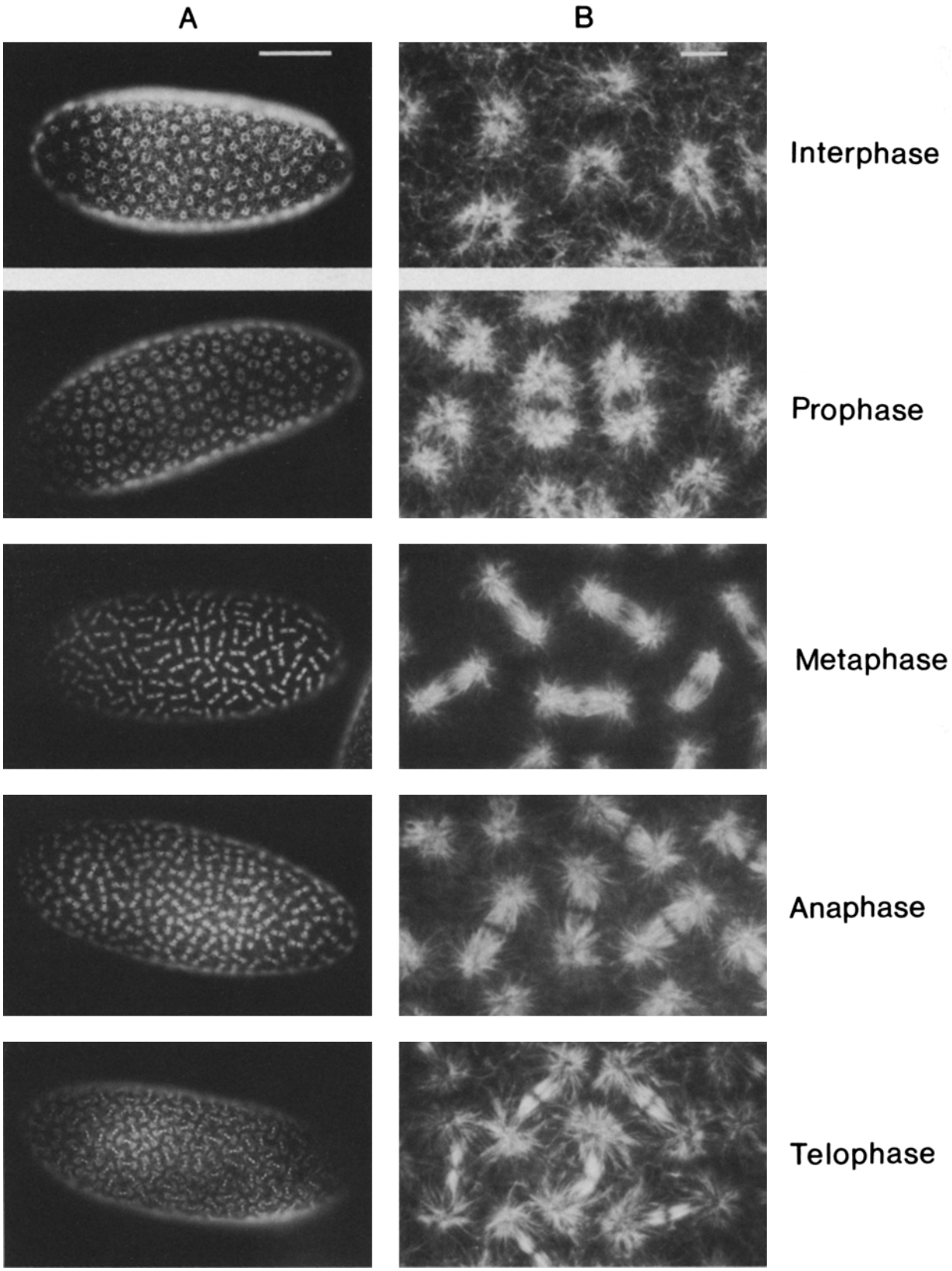

Figure 6. Changes in microtubule organization in *Drosophila* embryos during nuclear cycle 10. Stained embryos were photographed with rhodamine optics to examine their microtubule-containing structures. Both low (column *A*) and high (column *B*) magnification views of the microtubule-containing structures present during various stages of nuclear cycle 10 are shown. The cell cycle stage for each of the five embryos is given at the right of each pair of photographs, determined from the number of nuclei per embryo, the nuclear size, and the extent of chromosome condensation (not shown). For column *A*, bar denotes 100 μm; for column *B*, bar denotes 10 μm.

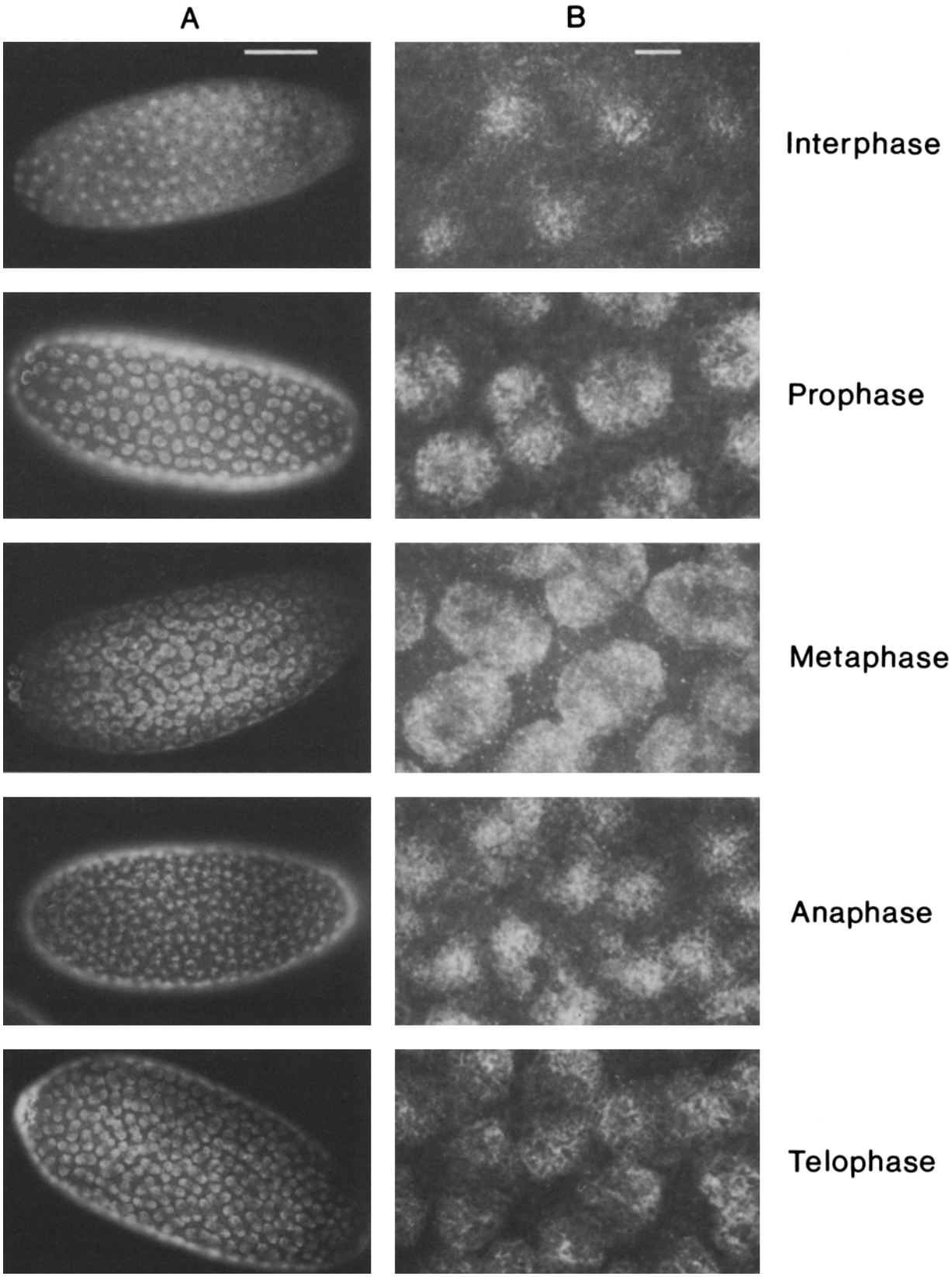

Figure 7. Changes in actin organization in *Drosophila* embryos during nuclear cycle 10. Both low (column *A*) and high (column *B*) magnification views of the actin-containing structures present during various stages of nuclear cycle 10 are shown. Embryos were photographed with rhodamine optics and staged as in Fig. 6.

The close correspondence between the spatial distributions of actin and tubulin at prophase is short-lived. By metaphase, nearly all of the detectable microtubules are in the spindle (Fig. 6, metaphase panels), while the actin forms a diffuse cap above the spindle that seems to delineate a distinct domain for each nucleus (Fig. 7, metaphase panels). Later, when the cycle 10 embryo progresses through anaphase and telophase, the spindle grows asters of increasing size from each of its two spindle poles (Fig. 6), as the spindle disassembles. The interphase array of microtubules is thus seen to be created from the large aster present at each spindle pole at telophase. Likewise, during anaphase, the actin appears to become concentrated around each spindle pole, thereby segregating half of the actin to the cap above each new interphase nucleus (see anaphase and telophase panels in Fig. 7).

Microtubules and Actin Filaments during Nuclear Cycles 11–13

As just described, nuclear cycle 10 represents a transition period during which global cytoskeletal reorganizations occur throughout the embryo. Since the next three cycles (cycles 11, 12, and 13) are essentially identical with respect to the behavior of actin, tubulin, and DNA, we will describe only nuclear cycle 11 in detail.

In Fig. 8, triple-label staining of five different embryos is shown, with the phase of the nuclear cycle indicated at the right. The columns display, respectively, the tubulin, actin, and DNA staining patterns, which are identical over the entire surface of the embryo except for the pole cells at the posterior pole. In general, the behavior of tubulin throughout nuclear cycle 11 is similar to that during nuclear cycle 10 shown earlier (Fig. 6). However, the actin staining patterns found during this nuclear cycle (and during cycles 12 and 13) are different in several respects.

As the nuclei leave interphase of cycle 11, the centrosome splits and the microtubules begin to form the mitotic spindle. The boundaries between adjacent cytoplasmic domains, which are seen as areas devoid of microtubule staining, become regions of contact between the enlarged actin networks associated with adjacent nuclei and, by prophase, a line of bright actin staining delineates the boundary between the closely spaced domains.

At metaphase, well-formed mitotic spindles are stained by the anti-tubulin antibody, with areas between spindles devoid of microtubule staining. The bright lines of actin staining now resemble a ring around each nucleus, with interlocking rings creating a distinct honeycomb pattern that extends over the entire embryo surface. The same pattern is found if fluorescent phalloidin is used to stain filamentous actin (48).

During anaphase, the marked growth of microtubules from the asters at the spindle poles is accompanied by an increase in the actin staining above each aster, and the brightly staining lines of actin between nuclei mostly disappear.

When mitosis ends, the nuclei enter interphase of cycle 12, shown in the bottom row of Fig. 8. Although the images of actin, tubulin, and DNA at each interphase are very similar, the adjacent cytoskeletal domains organized by each nucleus become smaller and more tightly packed together on the embryo surface as the number of nuclei doubles in each cycle.

A more detailed view of the interphase arrangement of actin and tubulin is shown in Fig. 9. The top row shows the filamentous nature of the actin overlaying each interphase nucleus, visualized with an anti-actin monoclonal antibody that yields clearer immunofluorescent images than the anti-actin polyclonal antibody used for most of the previous figures. Some of the neighboring actin domains are well-separated from their neighbors (Fig. 9 *a*). The bottom row shows the microtubule structures present in late interphase or early prophase. As interphase proceeds, there appears to be a tightening up of the cytoplasmic domain around each nucleus, and prominent areas devoid of microtubule staining are seen between adjacent domains (Fig. 9 *c*).

When interphase preparations similar to those in Figs. 8 and 9 are viewed at different focal planes, one finds that the actin is located farther from the nucleus than the tubulin. However, such information is best obtained by examining thin sections of the stained embryos, as shown in Fig. 10. The arrangement of tubulin (left panels) and actin (right panels) during interphase of cycles 10 and 11 is shown in the top and bottom rows, respectively. The majority of the microtubule staining is closely associated with the interphase nuclei, and it extends downward around each nucleus, as well as upward toward the plasma membrane. In contrast, most of the actin staining is located close to the plasma membrane, leaving the microtubule-rich area immediately above the nucleus devoid of actin staining.

In the sections shown in Fig. 10, *c* and *d*, cycle 11 embryos in metaphase have been stained to reveal either tubulin (left panel) or actin (right panel). All of the detectable microtubules are located in the brightly staining mitotic spindles, in agreement with the surface views shown earlier in Fig. 8 (tubulin, metaphase panel). Compared with interphase, two distinct changes in the actin organization can be seen. First, the actin layer present above each interphase nucleus has rearranged into a thinner but brighter layer of actin staining that is even more closely associated with the plasma membrane (Fig. 10 *d*). Second, this actin layer now extends downward from the surface into regions between adjacent mitotic spindles, presumably following the transient membrane furrows observed during each mitosis by Stafstrom and Staehlin (38). Thus, in whole mount preparations, the summation of images from multiple focal planes gives the false impression of a two-dimensional network of actin rings during mitosis (Fig. 8 and reference 48).

Discussion

Methodological Considerations

In this report we have described procedures suitable for the immunofluorescent examination, in both whole mount preparations and plastic sections, of the *Drosophila* embryo cytoskeleton. These methods have also enabled the locations of intermediate filaments (46; Walter, M., and B. M. Alberts, manuscript in preparation) and of several actin-associated and microtubule-associated proteins to be determined in these embryos (Miller, K., D. Kellogg, and T. L. Karr, unpublished results).

Unfortunately, embryo treatment with glutaraldehyde, the preferred fixative for microtubules, results in a high fluorescence background, necessitating the use of formaldehyde as the primary fixative. Our initial attempts to stain *Drosophila* embryos using the formaldehyde-based procedures developed

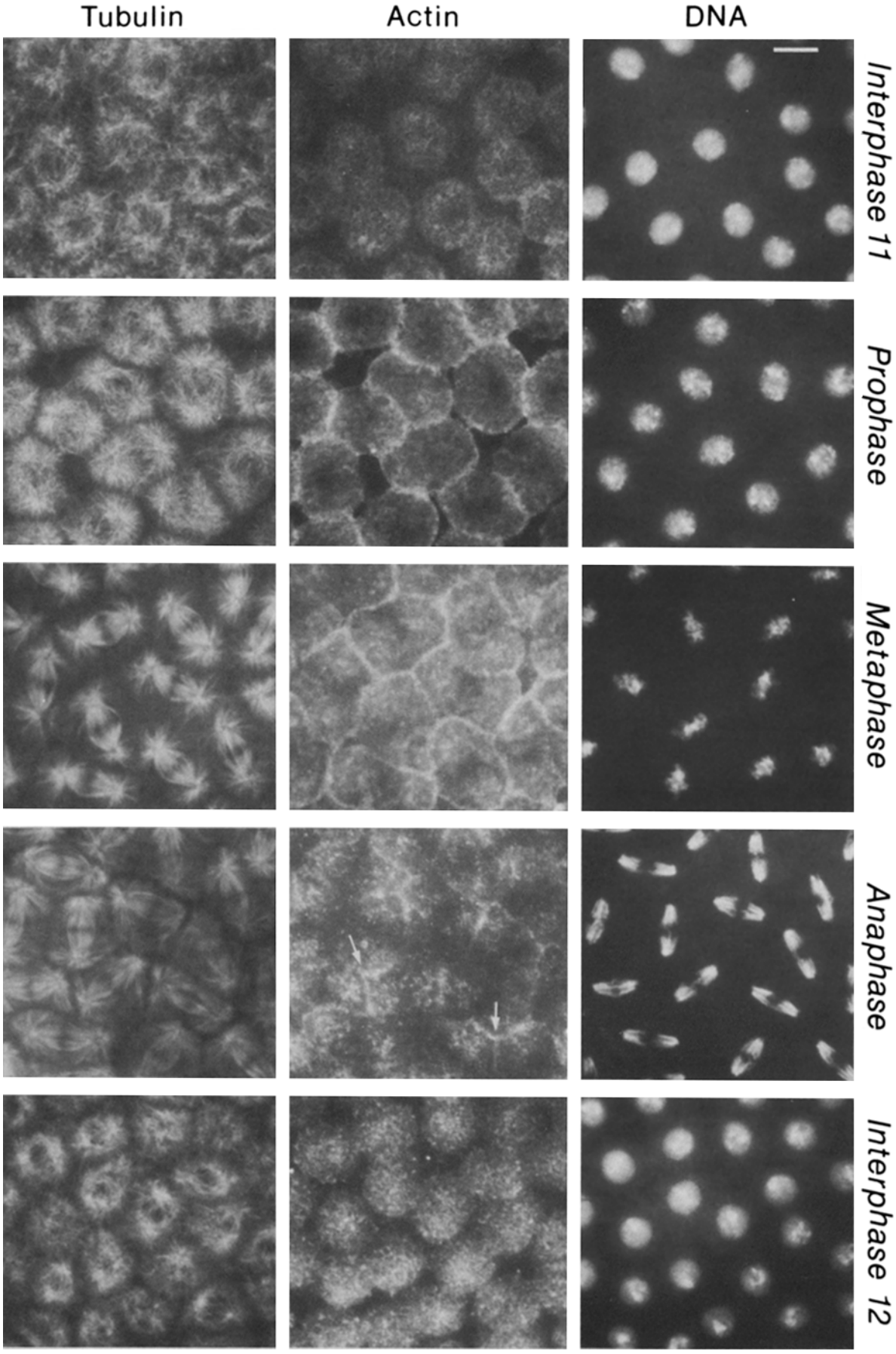

Figure 8. Cytoskeletal changes during the transition from nuclear cycle 11 to nuclear cycle 12. Pictured are the tubulin, actin, and DNA structures present during various times of development (labeled in the right margin), beginning at interphase of cycle 11 and ending with the subsequent interphase of cycle 12. Each horizontal row displays three fluorescent images obtained from one embryo that was stained for triple-label microscopy as described in Materials and Methods and viewed with fluorescein optics (tubulin), rhodamine optics (actin), or Hoechst optics (DNA). In the anaphase panel, arrows point to residual bright lines of actin staining that have not yet disappeared. Bar, 10 μm.

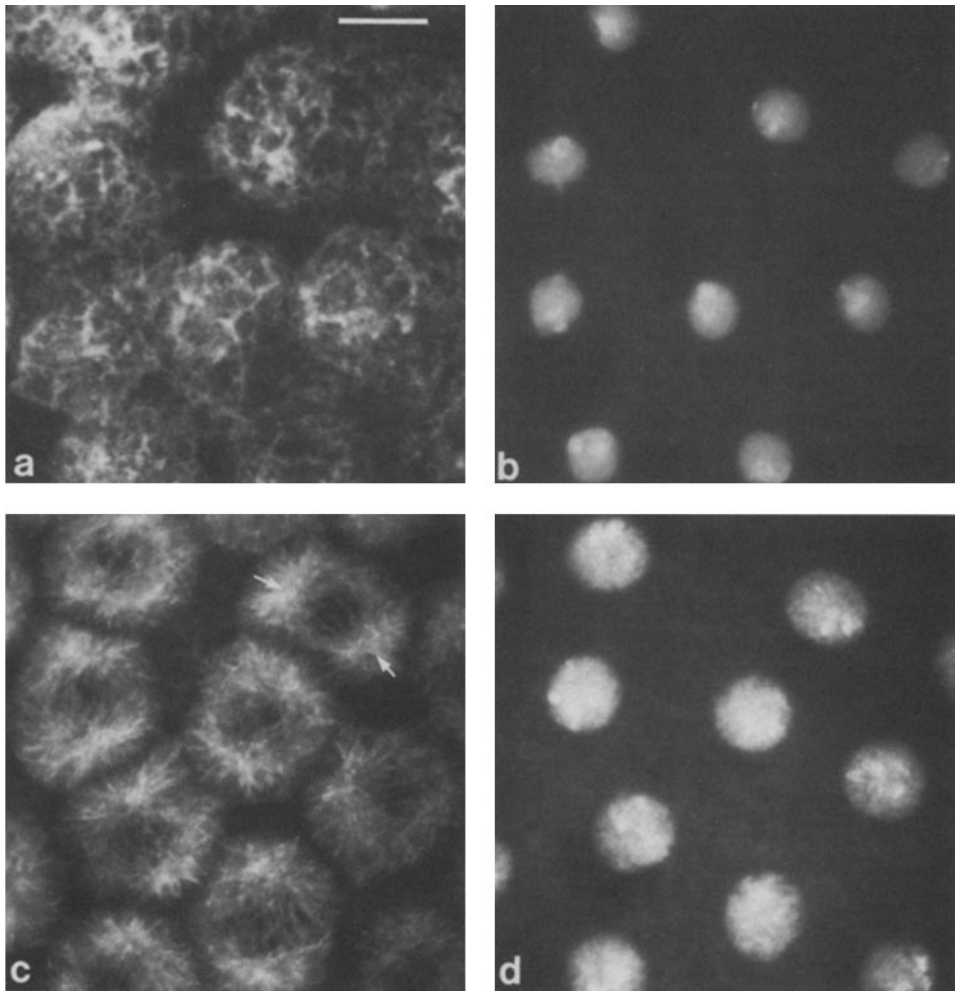

Figure 9. The actin and tubulin structures associated with nuclei at interphase of cycle 11 viewed at high magnification. (*a* and *b*) The filamentous actin-containing structures (*a*) that lie above the nuclei (*b*) during early interphase of cycle 11. (*c* and *d*) The microtubule-containing structures (*c*) surrounding the nuclei (*d*) present in an embryo ~3 min older than the embryo in *a* and *b*. As judged from its nuclear size and morphology, this embryo is just entering prophase and the arrows in *c* denote the presumed positions of recently separated centriole pairs. Microtubules emanating from such organizing centers cross over and around the nuclear envelope. Bar, 10 μm.

in the laboratory of J. Sedat (6, 25) failed to reveal any recognizable microtubules. We then found that the inclusion of taxol immediately before fixation results in clear immunofluorescent images of microtubules, as documented in Fig. 2. We have obtained the best cytoskeletal preparations when taxol is present for 15–30 s after the start of heptane permeabilization, just before the addition of formaldehyde. We suggest that during this brief period taxol penetrates the vitelline and plasma membranes, thereby binding to microtubules to stabilize them before the harsh conditions of fixation are encountered. Taxol has no noticeable effect on the actin staining in embryos; in addition, pretreatment of embryos with the actin-filament stabilizing drug, phalloidin (10 μg/ml for 1 min), did not appear to help to preserve actin filaments in our embryos (Karr, T. L., unpublished data).

Compared with other studies, the taxol level used in our fixation procedure (0.5–1.0 μM) is very low (5, 10, 22). For example, treatment with 10–20 μM taxol for a prolonged period was needed to induce small microtubule asters in the eggs of *Xenopus* (13) and sea urchins (34). We have tested the effect of increasing the taxol concentration and/or the incubation time before formaldehyde addition, using taxol concentrations as high as 12 μM and times as long as 5 min. Even under the most extreme conditions we find little change in the microtubules observed; the main effect of a 5-min incubation is the trapping of many embryos in anaphase (data not shown). It therefore seems reasonable to conclude that the main effect of taxol under our normal fixation conditions is to preserve pre-existing microtubule structures, although we cannot rule out the possibility that a small amount of microtubule growth occurs.

In this study rabbit polyclonal and mouse monoclonal antibodies produced against actin and tubulin from species distantly related to *Drosophila* were used for immunofluorescence analyses. The strong species cross-reactivity observed in Fig. 1 is not surprising, since actin and tubulin from species as divergent as yeast and chicken display ~75% amino acid sequence homology (2). In addition to the three antibodies described, we have also used a variety of other monoclonal and polyclonal antibodies against both actin and tubulin, and these have produced identical staining patterns to those reported here.

The Cortical Network of Actin and Tubulin in Early Embryos Is Rearranged after Nuclei Populate the Surface

Fig. 3 suggests that the cortical region of *Drosophila* eggs and early embryos contains considerable amounts of tubulin, in the form of microtubules, and actin. Low magnification views of whole mounts reveal that both actin and tubulin are distributed over the entire surface. Some of the actin is found in the form of punctate structures that underlie the plasma membrane to a depth of ~3–4 μm, but whole mount prepa-

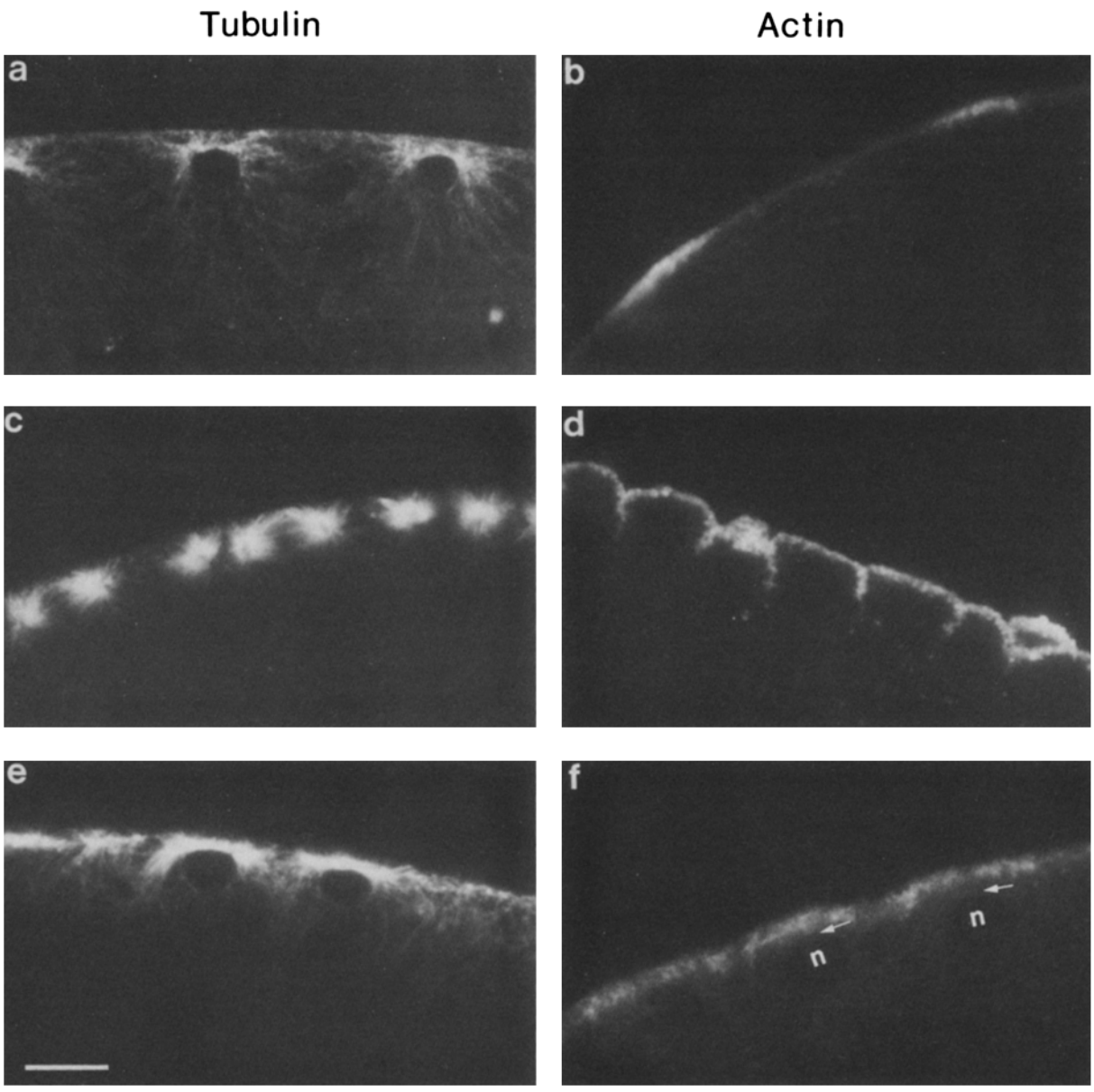

Figure 10. Sections of embryos stained to reveal either actin or tubulin during nuclear cycles 10 and 11. Embryos were fixed and stained to reveal either actin or tubulin structures, using rhodamine-labeled goat anti-mouse IgG as the secondary antibody. The stained embryos were then embedded in EPON and sectioned as described in Materials and Methods. Sections that contained appropriately staged embryos were examined with rhodamine optics and the images recorded. Shown are tubulin (*a*) and actin (*b*) during interphase of cycle 10, tubulin (*c*) and actin (*d*) during metaphase of cycle 11, and tubulin (*e*) and actin (*f*) during interphase of cycle 11. Arrows in *f* point to regions above the nuclei which correspond to the sites where the microtubule staining is most intense. Bar, 10 μm.

rations reveal a diffuse actin staining in addition to the punctate actin structures. The cortical layer of microtubules is also 3–4 μm deep. Due to the high concentration of these microtubules, their overall organization is difficult to ascertain; however, one can often observe small aster-like structures interspersed among the microtubules (see arrowhead in Fig. 3). The nature of these putative microtubule-organizing centers is unknown.

The signals that profoundly change the distribution of microtubules in the interior of the early embryo during mitosis appear to act only locally. Thus, the cortical cytoskeleton undergoes no noticeable alterations as the nuclei divide during the early cleavage stages. In contrast, there is a dramatic reorganization of the cortical cytoskeleton as the outward-migrating nuclei populate the surface to form a blastoderm during cycles 9 (pole cell nuclei) and 10 (somatic nuclei). The microtubules in the cortical regions appear to be reorganized to help form the extensive network around each nucleus. In addition, an actin "cap" appears directly above each somatic nucleus when it reaches the surface (Fig. 7 and reference 48). Thus, each nucleus would appear to be closely associated with an organizing center for both actin and tubulin.

The Importance of the Centrosome in the Organization of the Cytoskeletal Domain Around Each Nucleus

As determined by electron microscopic studies of *Drosophila* embryos (38), in early interphase a single centrosome (the

region surrounding and including the centriole pair) is located directly over each nucleus between the nuclear envelope and the egg plasma membrane. The two centriole pairs then move apart, remaining close to the embryo surface as they separate. The spindle forms between the two moving centrosomes during prophase, and prometaphase begins when the nuclear envelope is penetrated by spindle microtubules near the two spindle poles. The two centrosomes continue to move apart and drop deeper into the egg, until at metaphase they are positioned on opposite sides of the original nucleus. At the end of telophase, each newly reformed daughter nucleus rotates by 90 degrees, thereby restoring the early interphase orientation of the nucleus (9), and, by inference, the interphase position of the centrosome.

It is clear that the centrosome acts as an important organizing center for microtubules in *Drosophila* embryos, as expected from observations made in many other types of cells. More surprisingly, our results suggest that the centrosome, presumably by virtue of its microtubule-organizing activity, can also act as an important organizing center for actin. The first dense network of actin is organized in the cortex as a small spot under the plasma membrane, located at a point immediately above the centrosome associated with each early cycle 10 nucleus (Fig. 5, interphase). This actin spot quickly enlarges, and very soon becomes noticeably bipolar in appearance along with the microtubule network, as the centrosome splits at prophase (prophase, Figs. 6 and 7). By metaphase (Fig. 7), the actin network has spread out further, while retaining a bipolar organization that is co-oriented with the spindle.

The centrosome and its associated microtubules appear to continue to dictate the behavior of actin through the end of cycle 10. During anaphase chromosome movements, the actin domains seem to segregate with the astral microtubules that rapidly grow from the centrosome at each spindle pole (Figs. 6 and 7, anaphase panels). This type of actin behavior during cycle 10 has no obvious correlate in the mammalian cell, where the actin cytoskeleton has been examined in most detail. While our observations to date are only descriptive, they raise the question of whether a centrosome can organize cortical actin through microtubule–actin interactions.

The behavior and organization of actin seem to change between cycle 10 and cycle 11, since during mitosis of cycles 11, 12, and 13 the actin cytoskeleton is positioned in a way that appears to be less influenced by centrosomes, as summarized schematically in Fig. 11. This figure reviews the relative distributions of actin and tubulin at successive times as they would appear in the same embryo, starting with interphase of cycle 11 and finishing at the following interphase of cycle 12. Although an actin cap is located above the centrosome during interphase, when the centrosome splits the actin network under the plasma membrane (shown as dots) spreads out and begins to move into furrows between the newly forming spindles (thin lines), rather than following the centrosome microtubules as in cycle 10. Because this type of actin behavior begins in cycle 11, we suggest that the first membrane furrows appear in this cycle, re-occurring in each subsequent mitosis before cellularization.

Using fluorescently labeled phalloidin, which labels only filamentous actin, Warn and co-workers (48) have described similar actin filament structures during cycles 11–13. A fluorescent cell membrane marker (rhodamine-labeled concanavalin A) was used by these investigators in double-label immunofluorescence experiments to demonstrate close interactions between the plasma membrane and the actin filaments, in agreement with our results in Fig. 10.

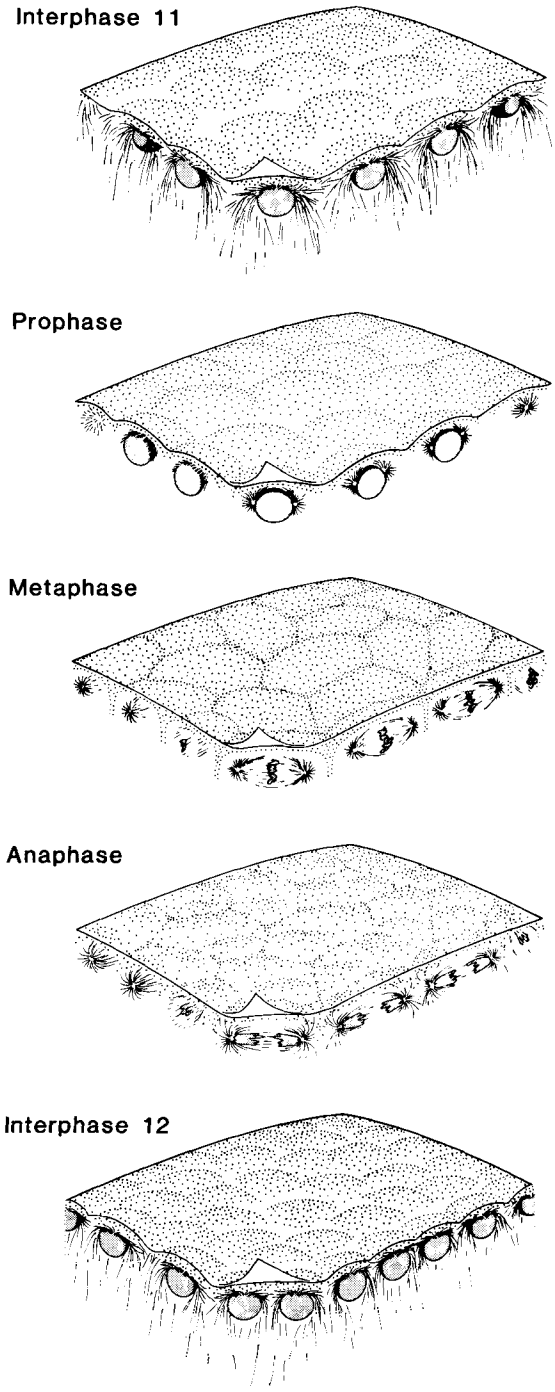

Figure 11. Schematic representation of the actin and tubulin structures observed in this study. This perspective drawing is a summary of our observations of immunofluorescently stained whole mount and sectioned preparations of *Drosophila* embryos (see Figs. 8 and 10 for examples). Each panel presents the organization of actin (dots), tubulin (lines), and DNA (gray stippling) during the indicated portion of nuclear cycle 11 or 12. A square section of the syncytial blastoderm surface that measures ~50 μm × 50 μm is illustrated (see Discussion).

Correlation with Functional Studies

Highly regulated temporal and spatial changes in the cytoskeleton have been associated with a number of processes in cultured cells (23, 49). However, our knowledge of cytoskeletal organization in developing embryos is far less extensive. Concerted and directed movements of egg contents is recognized as a ubiquitous occurrence in embryogenesis (4, 19, 33). In *Xenopus*, a microtubule-directed shift in the cytoplasm in the animal hemisphere has been shown to play an important role in the early determination of dorsal-ventral polarity (42). More relevant to *Drosophila*, in the gall midge *Wachtiella*, the migration of nuclei to the egg surface appears to depend on the structural integrity of microtubules. Here, long arrays of microtubules radiate from the spindle poles during anaphase and telophase and appear to mediate outwardly directed tractive forces on each nucleus and its associated cytoplasm (50).

In *Drosophila*, both colchicine and cytochalasin B have profound effects on development (8, 52). In permeabilized embryos, colchicine treatment before cycle 9 blocks nuclear migration, whereas treatment during the syncytial blastoderm stages blocks the characteristic thickening of the cortical cytoplasm that occurs during this time (52). The latter result implicates the arrays of microtubules seen in Fig. 10 in the organization of the entire zone of cytoplasm in the cortical region.

Cytochalasin B treatment of permeabilized *Drosophila* embryos before cycle 9 has been reported to allow continued nuclear divisions, but to inhibit the movement along the anterior-posterior axis that causes the early nuclei to become evenly distributed in the core of the embryo (52). As we have not yet detected actin filaments in the embryo interior, we are unable to connect this observation with our results. However, cytochalasin B treatment during the syncytial blastoderm stages results in "colliding mitoses" (52), which suggests that the furrows that normally separate adjacent spindles (38) may be absent. Similarly, injection of cytochalasin B into cycle 14 embryos disrupts the membrane furrowing process associated with cellularization (8).

We conclude that the actin we observe in close association with plasma membrane furrows (Figs. 8 and 10) is required for the furrowing process. As postulated for the furrowing process during cellularization (11, 47), an actin- and myosin-containing structure that resembles the contractile ring (35) may cause the transient invagination of the plasma membrane observed during mitosis in nuclear cycles 11, 12, and 13. The involvement of microtubules in the establishment of these transient membrane furrows cannot be evaluated at this time. However, by analogy with the extensive studies done in marine invertebrate eggs (reviewed in reference 30), it is reasonable to suggest that microtubule-mediated interactions with the plasma membrane in areas between closely spaced spindles could be involved in the establishment of the furrow.

The Two Regions of "Structured Cytoplasm" in Early Embryos Are Highly Enriched in Cytoskeletal Filaments

The nuclei that divide in the interior of the *Drosophila* embryo before nuclear migration have been known for many years to create a special clear domain of cytoplasm around them, which extends for ~30 μm from the center of each nucleus and excludes the surrounding yolk and other readily visible particles (4, 29, 36). Before nuclear migration a cortical layer of cytoplasm, ~3 μm deep beneath the plasma membrane, likewise excludes such particles (4, 36). We have previously referred to such cytoplasmic domains as "structured cytoplasm" (8) to differentiate them from much of the remaining egg contents, which at the present state of our knowledge would seem to be less organized.

Most cells seem to contain a special zone of cytoplasm just beneath their plasma membrane that excludes large particles. The simplest way in which such a special region of cytoplasm could be created is by the accumulation of a dense network of cytoskeletal filaments that physically excludes the particles. Mammalian macrophages contain a fine meshwork of actin filaments in their cortical cytoplasm that has been suggested to play such a role (39). The cortical region of *Drosophila* embryos not only contains a dense meshwork of actin and microtubules (Fig. 3), but also intermediate filaments (46). Because the filament-rich layer just beneath the egg plasma membrane and the clear region of cytoplasm detected in histological sections extend to the same depth (~3 μm), the above "filament exclusion" model seems quite reasonable.

What about the second region of structured cytoplasm in these embryos, that which surrounds each nucleus? Our studies show that the cytoplasm that surrounds the interphase nucleus is highly enriched in microtubules, both before and after nuclear migration (e.g., see Figs. 3 *e*, 6, and 10). However, when the nuclei are migrating outward to the surface, they create an extensive region of structured cytoplasm behind them that resembles the tail of a comet (36). In contrast, the microtubules that we detect in association with such nuclei are densely packed only on the side of the nucleus closest to the plasma membrane (Fig. 3 *e*). Thus, additional cytoskeletal proteins, including perhaps both microtubule-associated proteins and actin, could be involved in creating this special type of cytoplasm. Although actin filaments appear by immunofluorescence to be restricted to the cortex in our experiments, this may reflect the difficulty of fixing such filaments in the embryo interior. Dissecting the exact molecular basis of the structured cytoplasm will clearly require further electron microscopic and biochemical studies.

Is Positional Information Stored in the Cortical Cytoplasm?

As mentioned in the Introduction, cell ablation (21, 43) and nuclear transplantation (15, 27) experiments indicate that, whereas the nuclei at cycle 10 are undetermined, by cycle 14 (i.e., the cellular blastoderm stage) each newly formed cell is determined as belonging to a given segment. For example, cells in the anterior region are destined to form head structures, whereas cells in the middle of the embryo will form thoracic segments. Embryo ligation experiments in *Drosophila* (26) as well as other insects (4) suggest that this patterning process occurs gradually through the syncytial blastoderm stages and depends upon interactions along the anterior-posterior axis. Recently, the transcript of a gene known to be involved in segmentation, *fushi tarazu* (ftz), has been detected in pre-cellularized embryos by in situ hybridization. Remarkably, this transcript begins to localize in a banded pattern in cycle 13 embryos, well before cells have formed (12). This result provides clear evidence at the molecular level that

important determinative processes occur in the syncytial cytoplasm of these giant multinucleate cells.

The conceptualization of embryonic development relies heavily on the postulate of developmental fields and positional information contained within these fields (18, 24, 51). Our data suggest a possible structural basis for such a field. In particular, it is tempting to speculate that important factors that act to inform nuclei of their relative position in the embryo have become localized in specific regions of the cortical cytoplasm before nuclear migration, attached to the cytoskeleton there. When the nuclei reach the cortex in cycle 10, these factors would become incorporated into the local cytoplasmic domains that surround each nucleus during cycles 10–14, providing an asymmetry that helps to initiate the determinative processes that culminate at cellular blastoderm. There is some experimental evidence to support this general view. When early embryos of the leaf-hopper *Eusclis* were highly deformed with respect to their anterior-posterior axis through the use of a micro-vise, many of the embryos could develop normally after being released at cellular blastoderm (45). As pointed out (45), only the two-dimensional continuity of the egg cortex was left relatively undisturbed by these manipulations.

In a similar vein, when centrifugation of eggs is used to stratify egg contents, there follows a gradual rearrangement of the egg components, and, in many cases the embryo can develop normally. For example, whereas the centrifugation of *Smittia* eggs can induce the formation of double abdomen embryos (16, 17), similarly treated *Wachtiella* embryos develop normally (4). A cortex rich in cytoskeletal elements, similar to the one we have described in *Drosophila*, may impart the structural integrity needed to maintain the proper position of putative pattern elements during such centrifugation experiments.

We wish to acknowledge the helpful advice received from Frank McKeon and Tim Mitchison on immunofluorescence methodologies and Mei Lie Wong for help with the sectioning of embryos. We also thank Drs. Thomas Schroeder, Victoria Foe, and Gerald Schubiger for their critical reading of the manuscript. Finally we acknowledge the skillful secretarial assistance of Kathleen Rañeses and Cynthia Cunningham-Hernandez.

T. Karr is a Fellow of the Jane Coffin Childs Memorial Fund for Medical Research. This investigation has been supported by grant GM23928 from the National Institutes of Health.

Received for publication 24 June 1985, and in revised form 10 November 1985.

References

1. Blose, S. H., D. I. Meltzer, and J. R. Feramisco. 1984. 10-nm filaments are induced to collapse in living cells microinjected with monoclonal and polyclonal antibodies against tubulin. *J. Cell Biol.* 98:847–858.

2. Borisy, G. G., D. W. Cleveland, and D. B. Murphy, editors. 1984. Molecular Biology of the Cytoskeleton. Cold Spring Harbor Laboratory, New York. 1–512.

3. Brinkley, B. R., S. H. Fistel, J. M. Marcum, and R. L. Pardue. 1980. Microtubules in cultured cells: indirect immunofluorescent staining with tubulin antibody. *Int. Rev. Cytol.* 63:59–95.

4. Counce, S. J. 1973. The causal analysis of insect embryogenesis. *In* Developmental Systems: Insects. Volume 2. Academic Press, Inc., New York. 1–156.

5. DeBrabander, M., G. Geuens, R. Nuydens, R. Willebrords, and J. De Mey. 1981. Taxol induces the assembly of free microtubules in living cells and blocks the organizing capacity of the centrosomes and kinetochores. *Proc. Natl. Acad. Sci. USA.* 78:5608–5612.

6. Dequin, R., H. Saumweber, and J. W. Sedat. 1984. Proteins shifting from the cytoplasm into the nuclei during early embryogenesis of *Drosophila melanogaster. Dev. Biol.* 104:37–48.

7. Elgin, S. C. R., and D. W. Miller. 1978. Mass rearing of flies and mass production and harvesting of embryos. *In* The Genetics and Biology of *Drosophila.* Volume 2a. M. Ashburner and T. R. F. Wright, editors. Academic Press, Inc., London, New York, San Francisco. 112–120.

8. Foe, V. E., and B. M. Alberts. 1983. Studies of nuclear and cytoplasmic behavior during the five mitotic cycles that precede gastrulation in *Drosophila* embryogenesis. *J. Cell Sci.* 61:31–70.

9. Foe, V. E., and B. M. Alberts. 1985. Reversible chromosome condensation induced in *Drosophila* embryos by anoxia: visualization of the interphase nuclear organization. *J. Cell Biol.* 100:1623–1636.

10. Fuchs, D. A., and R. K. Johnson. 1978. Cytological evidence that taxol, an antineoplastic agent from *Taxus brevifolia,* acts as a mitotic spindle poison. *Cancer Treat. Rep.* 62:1219–1222.

11. Fullilove, S. L., and A. G. Jacobson. 1971. Nuclear elongation and cytokinesis in *Drosophila montana. Dev. Biol.* 26:560–577.

12. Hafen, E., A. Kuriowa, and W. J. Gehring. 1984. Spatial distribution of transcripts from the segmentation gene *fushi tarazu* during *Drosophila* embryonic development. *Cell.* 37:833–841.

13. Heidemann, S. R., and P. T. Gallas. 1980. The effect of taxol on living eggs of Xenopus laevis. *Dev. Biol.* 80:489–494.

14. Hilwig, I., and A. Gropp. 1972. Staining of constitutive heterochromatin in mammalian chromosomes with a new fluorochrome. *Exp. Cell Res.* 75:122–126.

15. Illmensee, K. 1972. Developmental potencies of nuclei from cleavage, preblastoderm, and syncytial blastoderm transplanted into unfertilized eggs of *Drosophila melanogaster. Wilhelm Roux's Arch. Dev. Biol.* 170:267–298.

16. Kalthoff, K., P. Hamel, and D. Zissler. 1977. A morphogenetic determinant in the anterior pole of an insect egg: localization by combined centrifugation and ultraviolet irradiation. *Dev. Biol.* 55:285–305.

17. Kalthoff, K. 1979. Analysis of a morphogenetic determinant in an insect embryo. *In* Determinants of Spatial Organization, 37th Symp., Soc. Dev. Biol. S. Subtelney and I. R. Konigsberg, editors. Academic Press, Inc., New York. 97–126.

18. Kauffman, S. A. 1971. Pattern formation in the *Drosophila* embryo. *Philos. Trans. R. Soc. Lond. B. Biol. Sci.* 295:567–594.

19. Krause, G., and K. Sander. 1962. Ooplasmic reaction systems in insect embryogenesis. *Adv. Morphog.* 2:259–303.

20. Laemmli, U. K. 1970. Cleavage of the structural proteins during the assembly of the head of bacteriophage T4. *Nature (Lond.).* 227:680–685.

21. Lohs-Schardin, M., C. Cremer, and C. Nusslein-Volhard. 1979. A fate map for the larval epidermis of *Drosophila melanogaster:* localized cuticle defects following irradiation of the blastoderm with an ultraviolet laser microbeam. *Dev. Biol.* 73:239–255.

22. Manfredi, J. J., J. Parness, and S. B. Horwitz. 1982. Taxol binds to cellular microtubules. *J. Cell Biol.* 94:688–696.

23. McIntosh, J. R. 1983. The centrosome as an organizer of the cytoskeleton. *In* Modern Cell Biology. Volume 2. B. H. Satir, editor. Alan R. Liss, Inc., New York. 115–142.

24. Meinhardt, H. 1977. A model of pattern formation in insect embryogenesis. *J. Cell Sci.* 23:117–139.

25. Mitchison, T. J., and J. Sedat. 1983. Localization of antigenic determinants in whole *Drosophila* embryos. *Dev. Biol.* 99:261–264.

26. Newman, S. M., Jr., and G. Schubiger. 1980. A morphological and developmental study of *Drosophila* embryos ligated during nuclear multiplication. *Dev. Biol.* 79:128–138.

27. Okada, M., I. A. Kleinman, and H. A. Scheiderman. 1974. Chimeric *Drosophila* adults produced by transplantation of nuclei into specific regions of fertilized eggs. *Dev. Biol.* 39:286–294.

28. Osborn, M., and K. Weber. 1982. Immunofluorescence and immunocytochemical procedures with affinity purified antibodies: tubulin containing structures. *Methods Cell Biol.* 24:79–132.

29. Rabinowitz, M. 1941. Studies on the cytology and early embryology of the egg of *Drosophila melanogaster. J. Morphol.* 69:1–49.

30. Rappaport, R. 1973. Cleavage furrow establishment—A preliminary to cylindrical shape change. *Am. Zool.* 13:941–948.

31. Rickoll, W. L. 1976. Cytoplasmic continuity between embryonic cells and the primitive yolk sac during early gastrulation in *Drosophila melanogaster. Dev. Biol.* 49:304–310.

32. Russell, W. C., C. Newman, and D. H. Williamson. 1975. A simple cytochemical technique for demonstration of DNA in cells infected with mycoplasmas and viruses. *Nature (Lond.).* 253:461–462.

33. Sander, K. 1976. Specification of the basic body plan in insect embryogenesis. *Adv. Insect Physiol.* 12:125–238.

34. Schatten, G., H. Schatten, T. H. Bestor, and R. Balczon. 1982. Taxol inhibits the nuclear movements during fertilization and induces asters in unfertilized sea urchin eggs. *J. Cell Biol.* 94:455–465.

35. Schroeder, T. E. 1975. Dynamics of the contractile ring. *In* Molecules and Cell Movement. S. Inoue and R. E. Stephens, editors. Raven Press, New York. 305–332.

36. Scriba, M. E. L. 1964. Beeinflussung der fruhen Embryonalentwicklung von *Drosophila melanogaster* durch chromosomenaberrationen. *Zool. Jb. Anat. Bd.* 81:435–490.

37. Sonnenblick, B. P. 1950. The early embryology of *Drosophila melanogaster. In* Biology of *Drosophila.* M. Demerec, editors. John Wiley & Sons, Inc., New York. 62–167. Reprinted in 1965, Hafner, New York and London.

38. Stafstrom, J. P., and L. A. Staehlin. 1984. Dynamics of the nuclear envelope and of nuclear pore complexes during mitosis in the *Drosophila* embryo. *Eur. J. Cell Biol.* 34:179–189.

39. Stossel, T. P. 1983. The spatial organization of cortical cytoplasm in macrophages. *In* Modern Cell Biology. Volume 2. B. H. Satir, editor. Alan R. Liss, Inc., New York. 203–223.

40. Towbin, H., T. Staehlin, and J. Gordon. 1979. Electrophoretic transfer of proteins from polyacrylamide gels to nitrocellulose sheets: procedures and some applications. *Proc. Natl. Acad. Sci. USA.* 76:4350–4354.

41. Turner, F. R., and A. P. Mahowald. 1976. Scanning electron microscopy of *Drosophila* embryogenesis. I. The structure of the egg envelope and the formation of the cellular blastoderm. *Dev. Biol.* 50:95–108.

42. Ubbels, G. A., K. Hara, C H. Koster, and M. W. Kirschner. 1983. Evidence for a functional role of the cytoskeleton in determination of the dorsoventral axis in Xenopus laevis eggs. *J. Embryol. Exp. Morphol.* 77:15–37.

43. Underwood, E. M., F. R. Turner, and A. P. Mahowald. 1980. Analysis of cell movements and fate mapping during early embryogenesis in *Drosophila melanogaster. Dev. Biol.* 74:286–301.

44. Vogel, O. 1977. Regionalisation of segment-forming capacities during early embryogenesis in *Drosophila melanogaster. Wilhelm Roux's Arch. Dev. Biol.*182:9–32.

45. Vogel, O. 1982. Development of complete embryos in drastically deformed leaf hopper eggs. *Wilhelm Roux's Arch. Dev. Biol.* 191:134–136.

46. Walter, M., and B. M. Alberts. 1984. Intermediate filaments in tissue culture cells and early embryos of *Drosophila melanogaster. In* Molecular Biology of Development, UCLA Symposium on Molecular and Cellular Biology, New Series. R. Firtel and E. Davidson, editors. Alan R. Liss, Inc., New York. 263–272.

47. Warn, R. M., B. Bullard, and R. Magrath. 1980. Changes in the distribution of cortical myosin during the cellularization of the *Drosophila* embryo. *J. Embryol. Exp. Morphol.* 57:167–176.

48. Warn, R. M., R. Magrath, and S. Webb. 1984. Distribution of F-actin during cleavage of the *Drosophila* syncytial blastoderm. *J. Cell Biol.* 98:156–162.

49. Weber, K., and M. Osborn. 1979. *In* Microtubules. K. Roberts and J. Hyams, editors. Academic Press, Inc., New York. 279–313.

50. Wolf, R. 1978. The cytaster, a colchicine-sensitive migration organelle of cleavage nuclei in an insect egg. *Dev. Biol.* 62:464–472.

51. Wolpert, L. 1969. Positional information and the spatial pattern of cellular differentiation. *J. Theor. Biol.* 25:1–47.

52. Zalokar, M., and I. Erk. 1976. Division and migration of nuclei during early embryogenesis of *Drosophila melanogaster. J. Microbiol. Cell.* 25:97–106.